SAND2021-6903J

High-Fidelity Modeling of Breakdown in Helium: Initiation Processes and Secondary Electron Emission

Amanda M. Lietz[1,4], Edward V. Barnat[1], George R. Nail[2], Nicholas A. Roberds[1], Andrew S. Fierro[3], Benjamin T. Yee[1], Chris H. Moore[1], Paul G. Clem[1], and Matthew M. Hopkins[1,4]

[1] Sandia National Laboratories, 1515 Eubank Blvd. SE, Albuquerque, NM 87123, USA

[2] Klipsch School of Electrical and Computer Engineering, New Mexico State University, 1125 Frenger Mall, Las Cruces, NM 88003, USA

[3] Department of Electrical and Computer Engineering, University of New Mexico, 211 Terrace St. NE, Albuquerque, NM 87131, USA

[4] Authors to whom correspondence should be addressed: amlietz@sandia.gov, mmhopki@sandia.gov

Understanding the role of physical processes contributing to breakdown is critical for many applications in which breakdown is undesirable, such as capacitors, and applications in which controlled breakdown is intended, such as plasma medicine, lightning protection, and materials processing. The electron emission from the cathode is a critical source of electrons which then undergo impact ionization to produce electrical breakdown. In this study, the role of secondary electron yields due to photons (γ_{ph}) and ions (γ_i) in direct current breakdown is investigated using a particle in cell direct simulation Monte Carlo (PIC-DSMC) model. The plasma studied is a one-dimensional discharge in 50 Torr of pure helium with a platinum cathode, gap size of 1.15 cm, and voltages of 1.2-1.8 kV. The current traces are compared with experimental measurements. Larger values of γ_{ph} generally result in a faster breakdown, while larger values of γ_i result in a larger maximum current. The 58.4 nm photons emitted from He(2^1P) are the primary source of electrons at the cathode before the cathode fall is developed. Of the values of γ_{ph} and γ_i investigated, those which provide the best agreement with the experimental current measurements are $\gamma_{ph} = 0.005$ and $\gamma_i = 0.01$. These values are significantly lower than those in the literature for pristine platinum or for a graphitic carbon film which we speculate may cover the platinum. This difference is in part due to the limitations of a one-dimensional model but may also indicate surface conditions and exposure to a plasma can have a significant effect on the secondary electron yields. The effects of applied voltage and the current produced by a UV diode which was used to initiate the discharge, are also discussed.

I. Introduction

In a low temperature plasma, electrons can be emitted from an electrode surface by several processes: electric field emission and secondary electron emission (SEE) by incoming ions, excited states, fast neutrals, electrons, and photons. In a typical glow discharge, the SEE from ions and photons are expected to dominate and are the focus of this investigation. Previous studies have shown that the photoelectron yields (γ_{ph}) and ion-induced secondary electron yield (γ_i) can significantly influence the discharge dynamics and the resulting current traces [1, 2]. Because these secondary electron yields are important in the plasma dynamics, the selection of materials in contact with the plasma and the condition of their surfaces should be considered when designing a plasma source.

SEE can influence the efficacy of plasmas in many applications. For example, computational modeling of atmospheric pressure plasma jets has shown the importance of γ_{ph} in influencing the speed of ionization wave propagation [3]. SEE is critical in the performance of some plasma thrusters [4, 5]. Using electrodes with high secondary electron yields in plasma reactors has also been shown to improve the efficiency of volatile organic compound destruction [6].

Several studies have focused on determining secondary electron yields by combining experimental measurements with Paschen's law or numerical modeling. Phelps and Petrović conducted a detailed review of secondary electron yield measurements for Ar discharges, including SEE due to photons, ions, metastables, and fast neutrals [7]. For some materials, a "dirty" surface could reduce γ_i by as much as two orders of magnitude at the low ion energies typically found in low-temperature discharges. They also developed an analytical model to highlight the contribution of each of these sources in steady state discharges (in the low-current limit, where the electric field is uniform) as a function of the reduced electric field, *E/N*. For clean surfaces, below 80 Td, SEE due to photons is the primary source of electrons at the cathode in steady state, whereas above 80 Td, SEE due to ions is the primary source. For dirty metals, this transition occurred around 300 Td. Nikolić *et al*. extended this approach to higher current densities with a semianalytical model [8].

Marić *et al*. used measurements of the breakdown potential to determine $\gamma_{effective}$, which is the ratio of the total number of electrons emitted from the cathode to the flux of ions [9]. This includes electrons emitted from the cathode by all processes (including photons). For various noble gases with a stainless steel cathode, $\gamma_{effective}$ was between 0.01 and 0.2 for E/N = 10-10,000 Td. For low values of *E/N*, photoelectron emission is expected to be the dominant source of electrons. Daksha *et al*. used an approach that combined simulations and the ratio of optical emission at different phases of an RF discharge to determine γ_i of steel [10]. In this case, the *in situ* measurement of γ_i was in agreement with measurements of clean surfaces. Petrović *et al*. also used imaging of a direct current discharge combined with a hybrid plasma model and fit the results by adjusting γ_i [11]. Delgado *et al*. studied the secondary electron yield of liquid water for biomedical and environmental applications. They proposed that ion-induced SEE was the main source of electrons entering the plasma from the liquid surface, with a value of $\gamma_i \leq 10^{-5}$ [12].

In this paper, a particle-in-cell direct simulation Monte Carlo (PIC-DSMC) model is used to study the breakdown of He in a parallel plate reactor with a platinum cathode and is compared with experimental current measurements. The system is modeled in one dimension. The SEE due to ions and photons affect the breakdown on different timescales. The current as a function of time demonstrates qualitative agreement with the experimental data at several voltages, though there are some discrepancies which will be discussed. The geometry and setup are described in Sec. II, and the model description is in Sec. III. The modeling results, including comparisons with the experiments, are in Sec. IV. This includes the base case, the effect of applied voltage, the effect of γ_{ph} and γ_i, and the role of the current due to the UV diode. The concluding remarks are in Sec. V.

II. Experimental Setup

Two electrodes were placed in a vacuum chamber with a 1.15 cm gap between them, as shown in Fig. 1a. The cathode is platinum and 10.16 cm (4 in.) in diameter. The anode is 2.54 cm (1 in.) in diameter and contains a 1.5 cm hole covered in a dense mesh to serve as a conductive boundary that permits UV

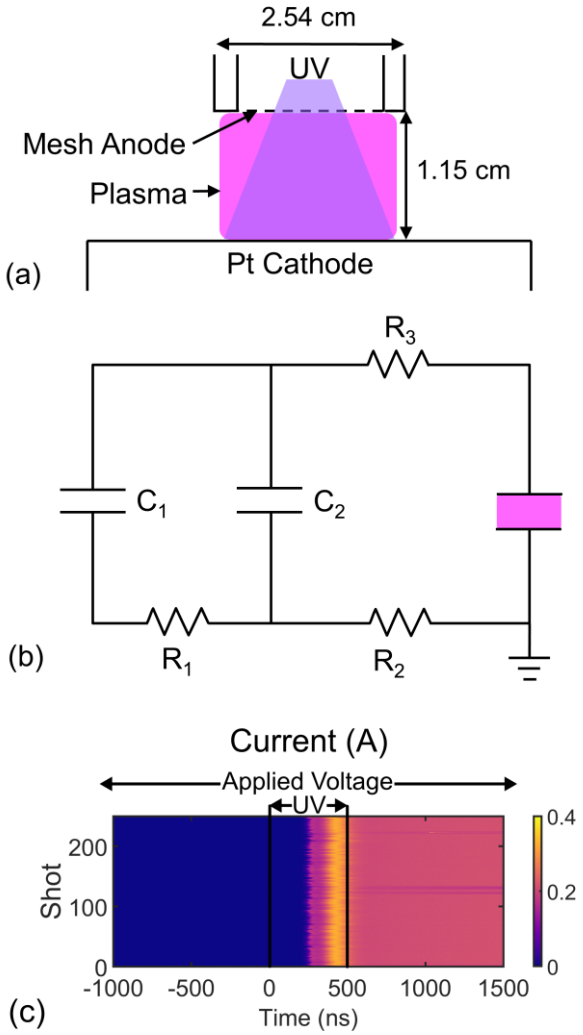

Figure 1. (a) The experimental setup of the one-dimensional plasma discharge which is the focus of this study. The anode is mesh to allow 265 nm light from a UV diode to illuminate the cathode, which initiates the breakdown. (b) The circuit used in the model. R_1 = 5 kΩ, R_2 = 10 mΩ, R_3 = 8.33 Ω, C_1 = 50 μF, C_2 = 40 pF. C_1 represents the power supply, and C_2 represents the measured stray capacitance in the experiment. (c) The current as a function of time for 250 shots of the experiment. The timing of the UV diode is also indicated.

photon transmission from a UV diode above the hole. The chamber is evacuated and filled with 50 Torr of ultra-high purity He (99.999% purity). A fixed voltage is applied to the anode. The UV diode is switched on at t = 0 s, and shines through the mesh of the anode, illuminating the cathode. The time sequence of the experimental setup, along with the measured current for each shot is shown in Fig. 1c. The voltage is on approximately 2 μs before the diode triggers the breakdown and remains on for 6 μs.

It was found that in the absence of the UV diode, the time delay for breakdown was much longer and highly variable between different discharge events. This stochastic behavior has also been observed by Pejović *et al.* and Maluckov *et al.* [13, 14]. However, rather than attempt to model the stochastic behavior which could be related to many physical processes (such as surface recombination [15] dependent on the state of the surface), the initiation variability was substantially reduced through the inclusion of the UV diode in both the experiments and the model. Illuminating the cathode with a diode provided a highly reproducible initiation time with negligible changes in the shape of the experimental current traces other

than the shift in time. By including a "trigger" source of initial photoemitted electrons we are able to make more definitive comparisons between experimental and model results without having the variability in the initial electron generation dominate the early discharge dynamics.

The UV diode light emits 265 nm (4.68 eV) light, which is less than the work function of Pt (5.7 eV). However, in practice it still provides a sufficient electron source to initiate the discharge. Though photoelectrons are not expected at this photon energy, it is possible that the broadening of the diode emission, reduced work function due to activation of the surface, a combination of the applied field and the photon flux, or imperfections on the surface enable photoelectron emission. This photoelectron emission is one difference between how the cathode surface in this experiment actually behaved and expectations from material characterizations found in literature for Pt or C (C was observed on the electrode surface in similar experiments). Although the cathode material did not behave according to those materials' properties, and we do not know the precise material properties, it did behave in a very reproducible manner. The current due to this UV photon flux alone was below detectable limits (expected to be on the order of μA).

The operating parameters of the experiment were selected to produce a quasi-one-dimensional discharge, provide a consistent time to breakdown, and eliminate any memory effects. The operating conditions in this geometry produced a cylindrical region of uniform plasma (e.g., no filaments). The voltage pulse duration was short enough, and the cathode was sufficiently large relative to the anode that the plasma never extended beyond the edges of the electrode. The discharge frequency was 0.1 Hz and the gas flow was ~350 sccm, which allowed sufficient time between discharges that the breakdown was independent of frequency (i.e., eliminating the memory effects). Some species can become adsorbed on the surface of the Pt from exposure to the environment (and may be removed by the plasma). To account for potential surface changes, the system was operated until the current trace no longer changed systemically from shot-to-shot. Therefore, we do not believe the cathode surface in this repetitively pulsed plasma was pristine Pt. Although the cathode did not behave as pristine Pt, the experiment did become strongly reproducible, as shown in Fig. 1c. For an applied voltage of 1.5 kV, the current reached a maximum value of 0.32 A and a steady state of 0.21 A.

III. Model Description

Aleph is a massively parallel electrostatic particle in cell direct simulation Monte Carlo (PIC-DSMC) model utilizing unstructured meshes and numerous advanced simulation capabilities. It is a Lagrangian method whereby a set of computational particles (each representing some number of real particles) is transported in an electric field (for charged particles). Interactions between particles are modeled with the DSMC method [16]. Here, we utilize a 1D3V implementation: particle positions are one-dimensional, but all three velocity components are retained. Poisson's equation is solved to provide electric potentials at the nodes of the unstructured mesh using the Amesos direct solver in the Trilinos library [17]. The charge density source term is aggregated from particle positions and charges. An electric field is derived from the electric potential solution and used in the force term applied to each charged particle. The following simulations, although one-dimensional, utilized 288-576 cores for 8-28 days, depending on the specific model parameters. This high computational cost for one-dimensional simulations is primarily due to the treatment of photons as particles, which limits the timestep of the simulation.

The DSMC method uses cross sections for reactions and collisions among particles. One advantage of the PIC-DSMC method is that there are no assumptions about the form of the velocity distribution functions; rather, their form is an outcome of the method. In the following simulations, photons are also treated as computational particles, enabling statistical photon transport calculations. This approach is important to accurately model the transport of photons from strongly self-absorbed transitions which have an absorption mean free path much shorter than the length scale of the plasma [18].

The experimental setup described in Sec. II was simulated in one dimension for pure He at 50 Torr. The computational mesh element size is 2.5 μm (4,600 cells). This mesh size resolves the Debye length and electron mean free path. It is also on the order of the mean free path for symmetric charge exchange of He^+. The voltage on the anode was determined based on a circuit model shown in Fig. 1b, with the current across the gap calculated using the method of Shockley and Ramo [19, 20]. This method accounts for the

displacement current resulting from charged species moving in the gap even if they do not contact an electrode. This method is required to calculate displacement current in an electrostatic PIC model, whereas it is naturally calculated in an electromagnetic PIC model. Before the simulation begins, a potential of 1 V is applied to the electrode of interest, and 0 V is applied to all other conductors. This setup is used to calculate a normalized reference value of the electric field throughout the domain, $\vec{E}_{SR}(\vec{x})$. The current into an electrode due to particle motion is

$$I = \sum_i \frac{\vec{E}_{SR}(\vec{x}_i)}{1\ \mathrm{V}} \cdot q_i \vec{v}_i \tag{1}$$

where $\vec{x}_i$ is the particle position, q_i is the particle charge, and $\vec{v}_i$ is particle velocity. This numerical approach allows the current to be calculated accurately even when changes in the electric field are many orders of magnitude less than the applied field.

The one-dimensional assumption approximates the plasma as a discharge between two infinite parallel plane electrodes. Any photons that are emitted in the gap contact the anode or the cathode. In reality a significant fraction of the photons are lost radially. We estimate in this case 60-80% of the photons may be lost radially. The charged and neutral species may also have some radial losses, though this would be small because the diffusion timescales are many orders of magnitude longer than the plasma lifetime. The one-dimensional assumption also results in an electric field that is only normal to the electrodes. In reality, there would be some field enhancement due to other components of the field in three dimensions.

The particle weights are not fixed, and dynamic reweighting was used, targeting 200 computational particles per cell for electrons, 100 for ions, and 50 for ground state He. Electronically excited states of He were reweighted with a target of 10 computational particles per cell. Particles are not cloned in reweighting, only merged, and a new particle is created at the center of mass of the two former particles. For neutral species, particles could be merged if their direction was within 90º and their speed was within 1.1 times the thermal speed. For charged species, in order for two particles to be merged their direction must have been within 30º and their velocities within 1 thermal speed, after accounting for the change in their energy when they are moved through the field to the center of mass. Reweighting was not applied to photons.

The minimum particle weight is applied such that one particle in the model is equivalent to at least one particle in the experimental setup. The simulation implicitly assumes that in one-dimension the cross-sectional area of the plasma is 1 m^2, which can be interpreted by applying a 1 m^{-2} factor to the particle weights. Therefore, the minimum particle weight was 1,974 m^{-2} (= $1/A_{\mathrm{plasma}}$, where A_{plasma} is the cross-sectional area of the discharge in the experiment, estimated from optical emission).

The photoelectron current due to the UV lamp (I_{UV}) was set at 27 pA, which is approximately 1 e^- every 6 ns, on average. In practice this means that at the beginning of the simulation the probability of emitting an electron at each timestep is $I_{UV}\Delta t/e$, where Δt is the timestep and e is the elementary charge. In the experimental data set, the current rise time had a standard deviation of 6 ns for 1.8 kV (the case with minimum variation). It is expected that this variance is due to the average time between electrons emitted from the cathode, plus some variance in the subsequent electron multiplication across the gap. Therefore 27 pA is the minimum possible current that could result in the 6 ns variation. The effects of this current will be discussed in Sec. IIID.

All electrons and ions recombined at the electrode surfaces, and all electronically excited states quenched. SEE was included for photons and He^+. Unless otherwise indicated, the secondary electron yields which provide the best qualitative agreement with the experiments were used: $\gamma_i = 0.01$, $\gamma_{ph} = 0.005$. γ_i was assumed to be independent of incident energy, based on measurements which show that it is approximately independent of energy below approximately 500 eV [7]. In the discharge regime of interest in this study, the electron and ion energies are typically not large enough for the kinetic emission of secondary electrons to provide a significant yield. Therefore, the electron-induced SEE is not significant. The ion-induced SEE is dominated by the potential energy (ionization energy) through Auger emission [21]. Secondary emission due to excited states was not included in the model because the fluxes of excited state neutrals are several

orders of magnitude lower than those of photons or ions. SEE due to He_2^+ was also excluded because He_2^+ densities are an order of magnitude less than that of He^+.

The reaction mechanism, which is a reduced version of that described in Fierro *et al*. [1], is available in the Supplementary Materials. The mechanism includes electrons, He^+, He_2^+, He_2*, all excited states for $n \leq 3$, and He(4^1P), with a total of 141 reactions, and 12 excited states. The reactions include electron elastic collisions, electron impact ionization, electron impact excitation, photon emission, photoexcitation, charge exchange, electron-ion recombination, associative ionization, and quenching of excited states. The only reactions that were removed from those in Fierro *et al*. [1] were those containing helium excited states with $n \geq 4$ except He(4^1P), which was retained in this mechanism. Attempts to further reduce the number of species resulted in significant differences in the current. The only addition to the mechanism described in Ref. [1] was the symmetric charge exchange of He^+ [22].

Though the spontaneous emission reactions were included for all species that radiate, only the photons from He(2^1P), He(3^1P), and He(4^1P) relaxing to the ground state are included as computational particles. These photons have enough energy to exceed the work function of Pt and are resonantly absorbed by the ground state. All other photons were assumed to be immediately lost from the domain and did not produce secondary electrons (but the state transitions are included). Based on recent studies, the contribution of photons from He_2* was assumed to be insignificant [3, 23].

Only photons with a mean free path greater than 50 μm were included in the model, using the method of Roberds *et al*. to reduce the computational intensity of tracking the most rapidly reabsorbed photons [24]. As each computational photon is emitted, it is assigned a wavelength from a distribution that accounts for natural, doppler, and pressure broadening [25]. An empirical model is used to determine the magnitude of doppler and pressure broadening [26]. The mean free path is calculated using the absorption cross section as a function of wavelength (which also includes natural, doppler, and pressure broadening):

$$\lambda_{mfp} = \frac{1}{N_g \sigma(\lambda_{photon})} \tag{2}$$

where λ_{mfp} is the photon mean free path, N_g is the number density of the ground state, and σ is the photoexcitation cross section of the ground state at a wavelength of λ_{photon}.

Photons which are close to line center have shorter mean free path and would be absorbed rapidly after emission. Excluding these photons is the equivalent of approximating them as being emitted and instantly reabsorbed at the same location. This method reduces the number of particles and allows a larger timestep because it limits the collision frequency of photons, which must be resolved. A timestep of 50 fs was still required to resolve the reabsorption of photons with a 50 μm mean free path, which have a mean absorption time of 170 fs. Because the photons are only absorbed by the ground state He, which is uniform, resolving the Courant-Friedrichs-Lewy condition for photons is not required (see Ref. [24] for details). Cutoffs of 20-50 μm were tested to confirm that 50 μm was an appropriate minimum mean free path. The 50 fs timestep also resolves the plasma frequency, the electron Courant-Friedrichs-Lewy condition, and the electron mean collision time.

To confirm the appropriateness of these numerical parameters, cell sizes from 0.4-2.5 μm, timesteps from 10-50 fs, and larger target particle counts per cell were all tested to determine that the parameters used were sufficient. For these tests, 5 different random number seeds were used for each condition to distinguish between stochastic and systemic differences.

III. Results

A. Base Case

The base case in this investigation refers to an applied voltage of 1.5 kV, and $\gamma_i = 0.01$, $\gamma_{ph} = 0.005$. The first electrons in the simulation are produced by the UV illumination of the cathode, which occurs stochastically. In this particular simulation, the first electron is emitted at $t = 4$ ns. As the initial electron at the cathode is accelerated in the electric field, the first electron impact ionization reaction occurs within 1 ns. Electron multiplication continues in this manner, leading to an electron density which grows exponentially across the gap (Fig. 2a). For this mesh (2.5 μm cells), a single particle corresponds to a density

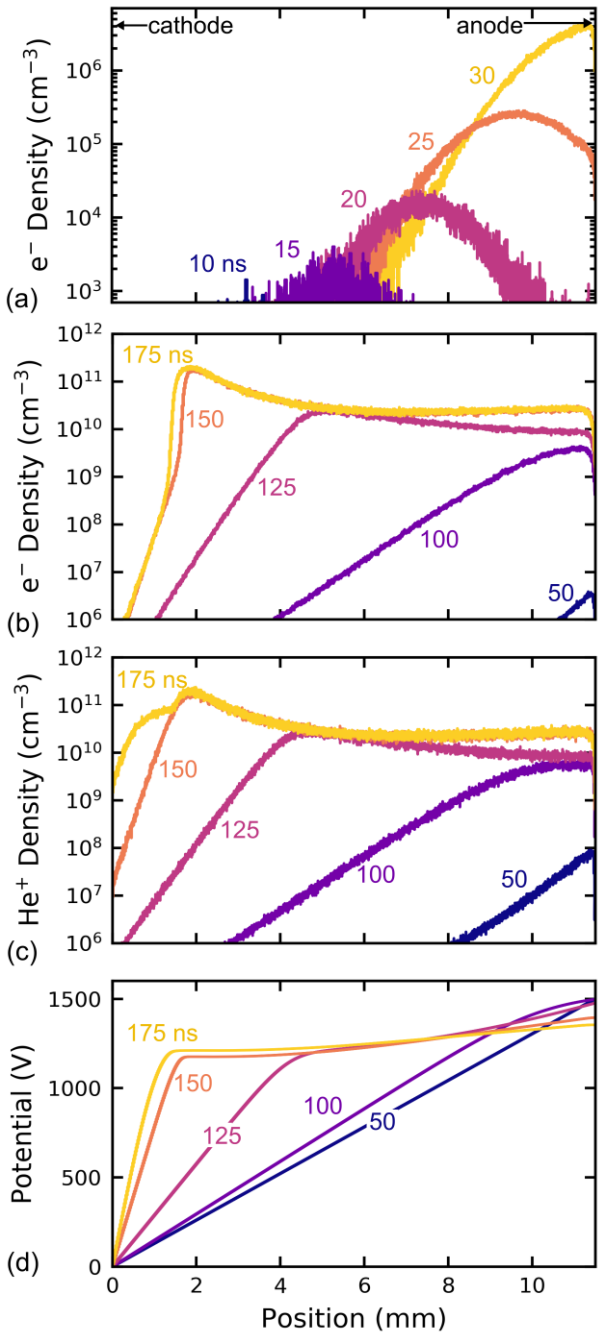

Figure 2. (a) The electron density as the first electron emitted from the cathode crosses the gap, undergoing electron impact ionization. The first electron emerged from the cathode at $t = 4$ ns. The time in ns is indicated on each line. The potential in the gap is unaffected by any space charge in the gas during this phase. (b) The electron density, (c) He^+ ion density, and (d) electric potential from the initial electron transit time to the development of a quasi-steady state glow discharge.

of 7.9×10^2 cm^{-3}. Over the course of this investigation, the first electron emitted from the cathode typically caused an avalanche, however, in a few cases a non-ionizing collision resulted in the electron backscattering and returning to the cathode and therefore did not cause breakdown. The time for the electron to transit the gap is approximately 30 ns. During the first 30 ns, the electron density does not exceed 5×10^6 cm^{-3}, and the space charge is not sufficient to significantly change the uniform electric field across the gap. The first

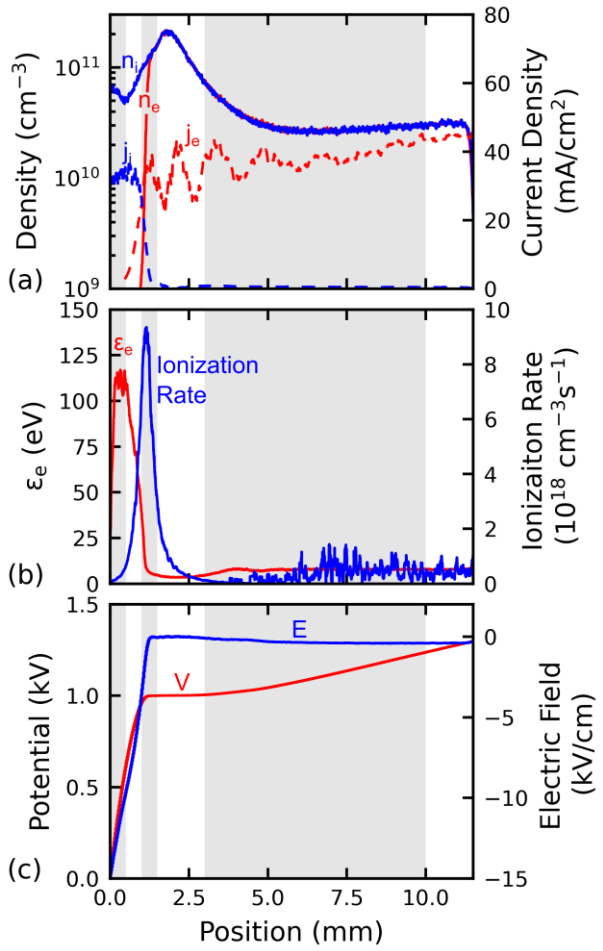

Figure 3. The plasma properties at 200 ns, after the cathode fall is developed. (a) The electron and ion densities (n_e, n_i), electron and ion current densities (j_e,j_i). (b) The average electron kinetic energy (ε_e) and the electron impact ionization rate of ground state He. (c) The potential (V) and electric field (E). The shading indicates the regions in which the electron and ion energy distributions are plotted in Fig. 4. (The data have been smoothed.)

discharge-generated photon contacts the surface at 20 ns, and the 200th photon contacts the surface by 30 ns. The first ion does not contact the surface until 89 ns, and the 100th photon contacts the surface at 134 ns.

After the initial electrons have drifted across the gap, the electron density continues to rise due to photoemitted electrons avalanching across the gap. After 65 ns the space charge begins to alter the potential in the gap. This positive space charge is a result of the more mobile electrons being accelerated out of the plasma faster than the ions, and is still relatively low (on the order of 10^7 cm^{-3}). The electron density near the anode increases until it reaches 5×10^9 cm^{-3} at 100 ns. At this point the region in which this density is elevated spreads from the anode toward the cathode, compressing the voltage drop into the region within 2 mm of the cathode. This region develops into the cathode fall by 175 ns. Initially, the electron and ion densities in this region are similar, but between 125 and 175 ns, the charge separation develops as the ion density increases and electrons are transported away from the cathode. After 125 ns, the voltage at the anode begins to decrease due to the increasing discharge current and corresponding increase in currrent through the series resistor (R_3 in Fig. 1b).

The plasma conditions with the developed cathode fall, shown in Fig. 3, are similar to that of a steady state classical glow discharge. However, in this case a steady state is not achieved during the simulation because as the current rises, the applied voltage begins to change according to the circuit, seen

in Fig. 3c where the voltage at the anode is no longer 1.5 kV. In the cathode fall, the ion density is 2-3 orders of magnitude larger than the electron density, and the electric field is large (~10 kV/cm, ~10^3 Td), so the ions carry most of the current. In the positive column (the bulk plasma), the electrons carry most of the current. The electric field in the bulk plasma is approximately 600 V/cm (37 Td). In a truly steady state direct current discharge, the displacement current is zero, and the formation of the cathode fall allows for current continuity. In this case, the sum of the conduction current densities, j_i and j_e, are not precisely constant across the gap due to the fact that the plasma is not at a steady state and the displacement current is non-zero. For example, there is a maximum in j_e of 45 mA/cm^2 near the anode which is greater than the cathode fall current density of 31 mA/cm^2.

The energy of the electrons increases as they are accelerated through the cathode fall, reaching average energies of 115 eV 0.3 mm from the cathode, as shown in Fig. 3b. The electron temperature, which excludes the energy associated with the bulk electron drift motion reaches its maximum of 40 eV at this same position. Although the average electron energy is high in the cathode fall, the electron density is low, so the rate of electron impact ionization is lower in this region than in the bulk plasma. The electron impact ionization rate of ground state He is 3×10^{16} cm^{-3}s^{-1} near the cathode, and increases exponentially until it reaches a peak of 9×10^{18} cm^{-3}s^{-1} at 1.2 mm. In the bulk plasma, the electron impact ionization rate of ground state He is approximately 5×10^{17} cm^{-3}s^{-1}. Eckert *et al*. discussed similar behavior in He at 200 Torr in the context of limitations of fluid models in addressing these electron energy distributions [27].

He(2^3S) is the most abundant excited state because it is has the lowest excitation energy and it is metastable. By 200 ns, the volume-averaged density of He(2^3S) is 6×10^{10} cm^{-3} and it continues to accumulate for the duration of the simulation. All of the other $n = 2$ states [He(2^1P), He(2^1S), He(2^3P)] have average densities that are a factor of 2 to 5 less than that of He(2^3S). The He_2* density remains negligible.

The normalized electron and ion energy distributions are shown in Fig. 4. Within 0.5 mm of the cathode, the electric field is largest (600-1000 Td) and the high energy tails of the electron and ion energy distributions are populated. Though most ions undergo many collisions as they traverse the cathode fall, a small fraction reach energies of 10^2 to 10^3 eV (note the log scale). These ions are expected to have a higher secondary electron yield, which would not be captured by the constant value of γ_i used in this model. However, because only 5% of the ions have an energy greater than 200 eV, the impact on the overall number of secondary electrons is expected to be minor.

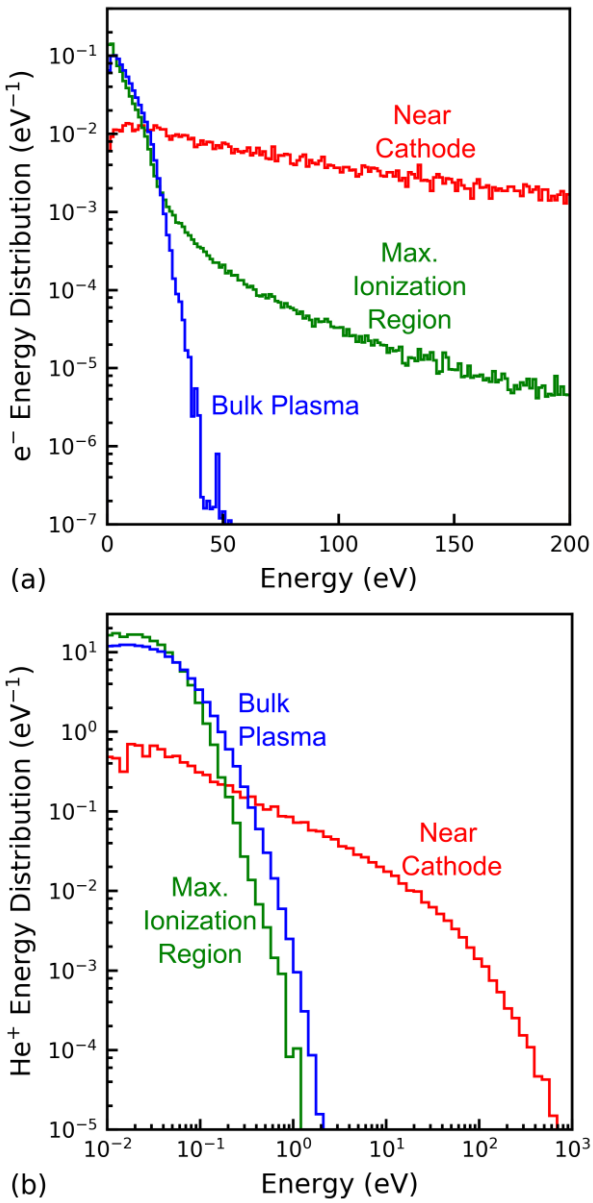

Figure 4. Histograms representing the (a) electron and (b) He^+ ion energy distribution in three regions of the discharge at 200 ns. The curves are normalized so that the integrated value is 1. "Near cathode" refers to the region $x < 0.5$ mm, "max. ionization region" refers to 1.0 mm $< x <$ 1.5 mm, and "bulk plasma" refers to 3.0 mm $< x <$ 10.0 mm. For electrons, energy is in a linear scale, but for ions, energy is on a log scale to show the different orders of magnitude in ion energy in different regions.

The region labeled "maximum ionization region" in Fig. 4 refers to the portion of the cathode fall which is closer to the bulk plasma and part of the negative glow, at 1.0 mm $< x <$ 1.5 mm. This region also has the highest ionization rate. The electric field in this region is lower than near the cathode, and the electron energy distribution is depleted in the tail above the threshold energy for ionization and other inelastic collisions which occur between 19.8 and 24.6 eV. In the bulk plasma, the high energy tail of the electron energy distribution is more than 2 orders of magnitude lower than in the region of maximum ionization. The ions in the region of maximum ionization are slightly less energetic than those of the bulk plasma. Many of these ions are generated in this region and have not yet been accelerated by the field (<

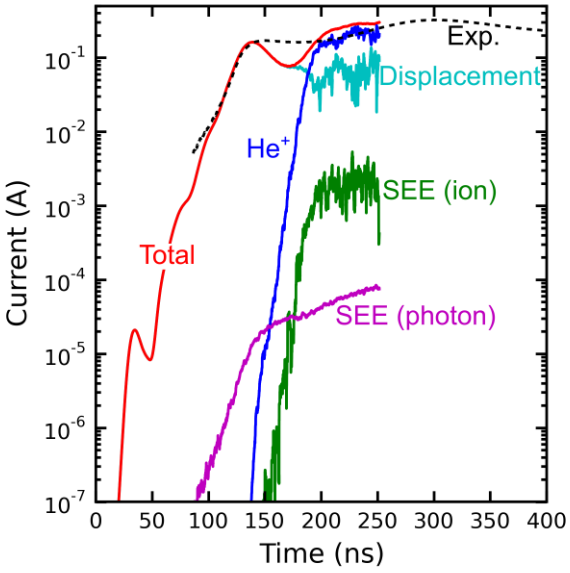

Figure 5. The total current (including displacement current) in the experiment and the model. Also shown from the modeling results are the current at the cathode due to the flux of He^+ ions and secondary electron emission (SEE) due to photons and ions. The displacement current was calculated by subtracting the He^+ and e^- currents from the total current. The current due to the UV diode is negligible (~10^{-11} A). The experimental current has been shifted left by 112 ns. Curves have been smoothed.

300 Td). Additionally, this region includes part of the negative glow, the region where the electric field is near to 0 kV/cm (see Fig. 3c).

Before the cathode fall develops and the ion current becomes significant, the emission of electrons from the cathode strongly influences the rate of rise of the current. The contribution of different sources to the total current at the cathode as a function of time is shown in Fig. 5. Note that the experimental current has been shifted left (earlier in time) by 112 ns. The total current includes the displacement current calculated using the method of Shockely and Ramo [20, 19], which should be analogous to the experimentally measured current. In many cases, the current reported in electrostatic PIC models is simply the net charge that impacts an electrode surface per unit time. However, this method ignores the displacement current which results from the net motion of charged species in the gap, which can change the electric field at the electrode surface. The current at the cathode is made up of the flux of ions into the cathode, the net emission of electrons from the cathode, and the displacement current. The current due to the UV diode (I_{UV} = 27 pA) provides the initial electrons, but quickly becomes negligible compared to the other sources.

In the first 30 ns, the total current increases exponentially as the initial electron multiplies across the gap, inducing displacement current at the cathode. Though the electric field in the gap does not undergo noticeable changes at this time, only miniscule changes in the electric field at the cathode are required to produce displacement currents below 10^{-4} A. For example, a displacement current of 10^{-5} A is equivalent to the electric field at the cathode changing by 1 V/cm over 50 ns (compared to an applied field of 10^3 V/cm). At 35 ns, the electrons from the initial avalanche (most of which are produced closer to the anode) exit the domain more rapidly than the ionization rate. When the total number of electrons decreases, the current due to the electrons moving in the gap decreases. This electron current in the gap corresponds to displacement current at the cathode which also decreases. This process causes a peak in the total current at 35 ns, followed by a decrease. However, photon-induced secondary electrons emitted from the cathode produce more electrons by electron impact ionization and cause the current to increase again within a few 10s of nanoseconds.

As shown in Fig. 5, the SEE due to discharge-produced photons initially rises exponentially, and provides the main flux of charged species at the cathode for the first 154 ns. During this period, the total current is approximately 4 orders of magnitude greater than the current due to the flux of charged species at the cathode. The majority of the current at the cathode is displacement current induced by the charged species in the gap changing the electric field at the cathode surface. Because electrons emitted from the cathode multiply across the gap, the electron flux is greater at the anode. Therefore the electron current is the main source of total current at the anode.

At 154 ns, the electric field near the cathode has reached approximately 10^4 V/cm, and the flux of ions toward the cathode exceeds that of the electrons leaving the cathode. With this comes an increase in ion-induced SEE, which exceeds the photon-induced SEE at 175 ns. Because $\gamma_i < 1$, the ion-induced SEE does not dominate the flux of charged species at the cathode at any point, but it is still a critical process. Electrons emitted at the cathode multiply by electron impact ionization in the high field of the cathode fall and produce the ions which are then accelerated back toward the cathode. The impact of this process will be discussed in Part C.

As the formation of the cathode fall approaches a steady state, the rate of change of the electric field at the cathode slows, causing a decrease in the displacement current. This results in the total current decreasing from 140 ns to 170 ns. There is a delay in the rise of the ion current as the ions, which are primarily produced by electron impact ionization at $x \geq 1$ mm (see Fig. 3b), drift through the cathode fall (see Fig. 2c). Though the majority of the ions do not reach the cathode until 190 ns, the small fraction of ions which are produced at $x \leq 1$ mm, or with above average energy begin to arrive in significant numbrs around 160 ns. This delay in the rise of the ion current causes the local minimum at 160 ns, after which the increasing ion current is a significant fraction of the total current.

Though the model captures the general behavior observed in the experiment, there are a few notable differences. In general, the dynamics in the model occur faster than that of the experiment. The experimental current measurement has been shifted left (earlier in time) by 112 ns to align the first peak in current. The development of the cathode fall and transition to ion-dominated current also occurs earlier in the model than similar features in the experimental current trace. The faster dynamics in the model could be caused by several factors:

a) The simplification of the problem to one dimension may cause the dynamics to occur more quickly. For example, in the model, all photons contact the cathode or anode, but in the experiment, some photons are lost radially. Including the radial losses could cause at least a factor of three reduction in the photon flux to the cathode. There may also be some spatial variations in the electric field due to the three-dimensional geometry allow some energy to transport laterally instead of only along x.
b) It was assumed that the effect of the UV diode is to produce electrons at the cathode, but it is possible that it actually causes ionization in the gas (perhaps of an impurity or residual excited state). In that case, the initial electron avalanches across only part of the gap, producing fewer excited states and fewer photons. Some initial tests have shown that this causes an 80 ns delay in the current rise which is on the order of the difference in the model and the experiment.
c) It was assumed that I_{UV} is constant at 27 pA (averaging 1 e^- every 6 ns), but it may increase over many ns, causing a delay in the emission of the first electron (on average). In a similar experimental setup, X-ray photoelectron spectroscopy measurements indicated that the platinum cathode surface was often coated with carbon. However, it could not be characterized *in situ* for these plasma conditions. Because the UV photon energy (4.7 eV) is most likely less than the work function, the process of electron emssion may be more complex than typical photoelectron emission. For example, perhaps the UV photons excite some impurities or adsorbed species on the surface, which are then ionized by a subsequent photon. After 10s of ns, there is a sufficient density of these surface excited states that emission of an electron becomes more likely. This could cause the probability of producing an electron on a given timestep to increase with time.

Two other explanations for the faster dynamics in the model were considered but eventually eliminated:

d) If the gas phase ionization rate (by ionization of the ground state or excited states) was overestimated in the model, we would also expect the initial current rise to be accelerated. However, the value of the

first Townsend coefficient, α, in the model was in agreement experimental measurements (Ref. [1] and the references therein), so we do not expect this to be the cause.

e) The inductance of the circuit could smooth the current, but this was deemed unlikely in some initial modeling tests. Even an inductance orders of magnitude larger than expected in this setup did not change the current trace significantly.

For currents below 10 mA, there is some deviation of the shifted experimental curve from the modeling results. However, these current measurements are only slightly above the noise, so there is less confidence in these than the rest of the experimental curve. The dip in current at 170 ns is exaggerated in the model compared to the experiment. In the model, the dip occurs when the current at the cathode is still dominated by displacement current, and the current begins increasing again as the flux of ions becomes a significant component of the current at the cathode. This may be caused by the cathode fall forming slightly faster or slower as a function of radius, violating the one-dimensional assumption. There is some uncertainty with all of the cross sections, and an overestimate of the symmetric charge exchange cross section for ions ($He + He^+ \rightarrow He^+ + He$) in the model could reduce the ion current and cause these effects.

B. Voltage

Three different values of applied voltage were tested in the experiment and the model, and the results are compared in Fig. 6. All curves are shifted to align a current of 30 mA to t = 0 ns. For the experimental measurements, this occurs at 801, 223, and 106 ns at 1.2, 1.5, and 1.8 kV. For the modeling results, this occurs at 609, 112, and 46 ns, though this is expected to vary depending on the random number seed. Although in all cases the breakdown occurs faster in the model than the experiment, the qualitative trends with varying voltage are captured. For all voltages, the dip in the current as the cathode fall forms is exaggerated in the model compared to the experiment, again possibly due to the one-dimensional assumption.

The time at which the ion current at the cathode exceeds the current due to photoelectron emission is 660, 154 and 76 ns for 1.2, 1.5, and 1.8 kV. With increasing voltage, electrons multiply more rapidly as they traverse the gap, resulting in a greater number of photons reaching the cathode (more $He(2^1P)$ is produced closer to the cathode). The larger photon flux increases the exponential growth rate of the current, as shown in Fig. 6. With higher voltage, there is more space charge in the gap and the cathode fall develops

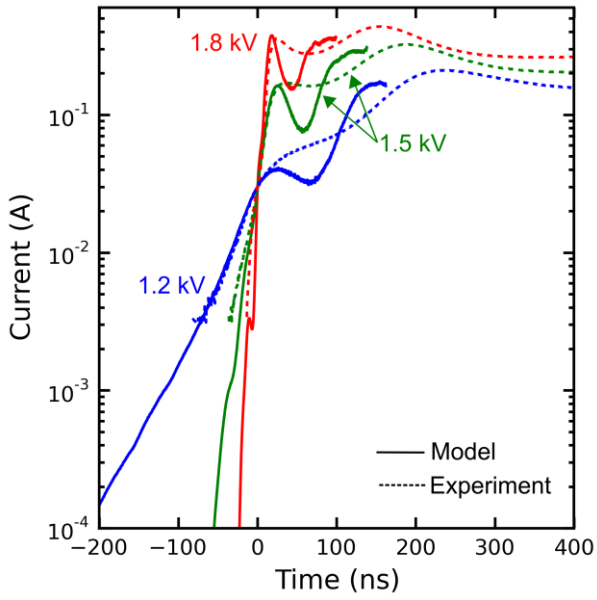

Figure 6. The total current (including displacement current) for different applied voltages. The time has been shifted to align t = 0 to 30 mA.

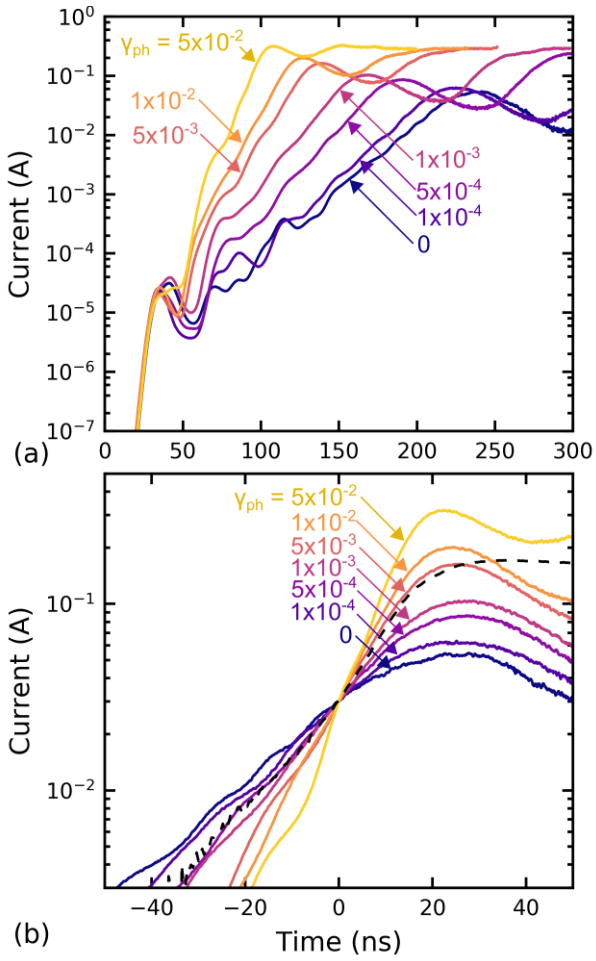

Figure 7. The current for different values of γ_{photon}.(a) Current calculated in the model for $\gamma_{ph} = 10^{-4}$, 10^{-3}, 5×10^{-3}, 10^{-2} (b) all curves shifted to align the current at 30 mA. $\gamma_i = 0.01$ in all cases. The experimentally measured current is the dashed curve.

more quickly, so *dE/dt* at the cathode is larger. Displacement current is the primary source of current at the cathode during the first current peak, so this peak is larger for higher voltages. As a result, the dip in total current as the cathode fall develops is more significant at higher voltage in both the experiment and the modeling results.

C. Secondary Electron Yields

Varying the secondary electron yields in the model highlights the impact of different electron emission processes at the cathode. It also provides insight on how the choice of electrode materials can impact the breakdown process and the rate of the current rise as breakdown occurs. The current trace with varying values of γ_{ph} are shown in Fig. 7. Because the random number seed was the same in each of these simulations (and the details of this model implementation), each simulation emits its first electron from the surface (due to I_{UV}) at 4 ns. In the base case, the first discharge-generated photon contacts the surface at 20 ns. However, changes in the calculated current due to γ_{ph} are not apparent until the current exceeds 10 μA (40 ns). The photon flux to the surface is primarily from He(2^1P). Photons from He(3^1P) and He(4^1P) are also included and can cause emission of photoelectrons, but their flux is generally < 2% of those from He(2^1P). The slope of the current in Fig. 7a, corresponding to the exponential growth rate of the current, increases with increasing γ_{ph}. The magnitude of the first current maximum exceeding 10 mA also increases with increasing γ_{ph}, from 0.05 A to 0.3 A for $\gamma_{ph} = 0$ to 5×10^{-2}. This maximum corresponds to when the

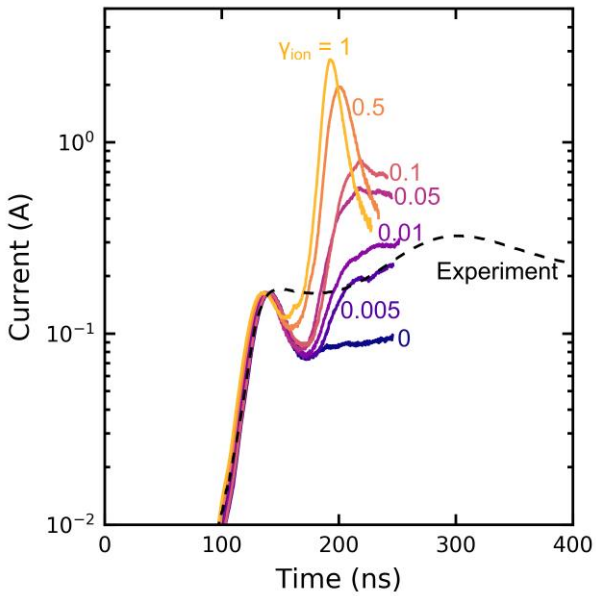

Figure 8. The current $\gamma_{ph} = 5 \times 10^{-3}$, $\gamma_i = 0$, 0.005, 0.01, 0.05, 0.1, 0.5 and 1. The experimentally measured current is the dashed curve. The experimental current has been shifted left 112 ns.

changes in the electric field at the cathode begin to slow as the cathode fall forms. In Fig. 7b, the current traces are all shifted so that 30 mA occurs at $t = 0$, as stated earlier, to better illustrate the variation in slope. $\gamma_{ph} = 5 \times 10^{-3}$ provides the best fit with the experimental slope of the values we tested. Although lower values of γ_{ph} better agree with the experimental time to reach 30 mA, fitting the slope is more physically connected to photoelectron emission. $\gamma_{ph} = 5 \times 10^{-3}$ is significantly lower than that of most estimates from literature which are typically greater than 0.01 [28]. The lower than expected value of γ_{ph} required to reproduce the experimental results may indicate an insufficiency of the model, such as the overestimation of the number of photons which reach the electrodes in one dimension. By approximating the view angle to the cathode at each point in the domain, it is estimated that the photon flux is overestimated by at least a factor of 3 due to radial photon losses. This overestimate is even more severe early in time when many of the photons originate near the anode. This indicates a value of γ_{ph} in the experiment may be closer to 0.01-0.03. The value of γ_{ph} also may be influenced by impurities or imperfections on the surface.

Because of the challenge and computational cost of including radiation transport in plasma models, photoelectron emission is often excluded. From the results in Fig. 7a, as γ_{ph} decreases, the rise time increases by approximately a factor of 2, but the change in maximum current is negligible. If γ_{ph} is ignored, it may still be possible to accurately capture the steady state or maximum current, but the rate of current rise would be incorrect. In some simulations which are always in a transient state, like plasmas driven by a pulsed or sinusoidal waveform, the photoelectron emission may also be important for capturing the steady state dynamics.

Simulations with $\gamma_{ph} = 5 \times 10^{-3}$ and different values of γ_i are shown in Fig. 8. Increasing γ_i increases the magnitude of the second peak in the discharge current but has a negligible effect on the current before 154 ns. The local minimum in the current which occurred at 170 ns in the base case shifts earlier in time and is not as low for higher values of γ_i. When γ_i is larger and more electrons are emitted from the cathode, more ions are produced in the cathode fall, and the ion current can rise more quickly. The maximum current also increases with γ_i from approximately 0.28 A for $\gamma_i = 0.01$ to 2.7 A for $\gamma_i = 1$, compared to 0.32 A for the experiment. This maximum occurs as the cathode fall forms and the ion flux to the cathode increases, but the applied voltage decreases due to the driving circuit.

To illustrate the effect of material properties on the breakdown dynamics, the experimental current trace and the base case modeling results were compared to simulations which use literature values of γ_{ph}

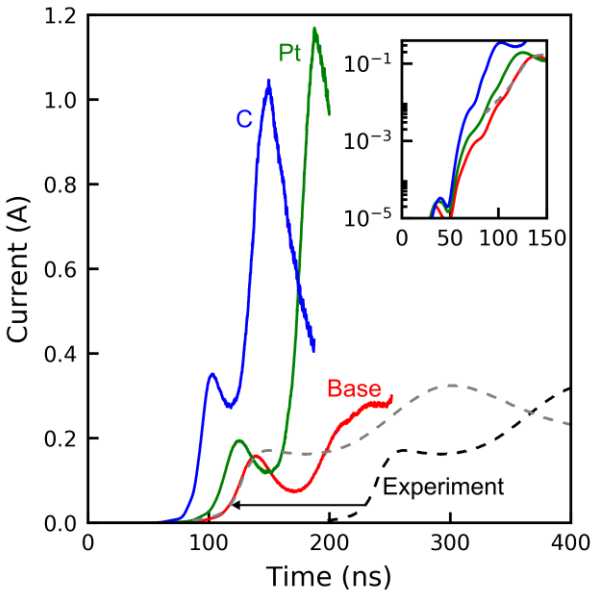

Figure 9. The current for 1.5 kV using the base case values (Base, $\gamma_{ph} = 5 \times 10^{-3}$, $\gamma_i = 0.01$), the literature values for Pt (Pt, $\gamma_{ph} = 0.01$, $\gamma_i = 0.21$), and the literature values of graphitic carbon (C, $\gamma_{ph} = 0.08$, $\gamma_i = 0.15$). The inset shows the same results plotted on a log scale. The experimental curve has been shifted by 112 ns to align it with the base case at 30 mA.

and γ_i [29, 30]. The results are shown with current on a linear scale and a log scale (inset) in Fig. 9. Note that the experimental curve in gray has been shifted by 112 ns to align with the base case at 30 mA. The literature values for Pt and C surfaces both cause more rapid rises in current and larger maximum values than are seen experimentally.

D. Initial electron flux

The flux of electrons from the cathode due to the UV lamp (I_{UV}) can influence the time to breakdown, as shown by the modeling results in Fig. 10. Increasing I_{UV} does not change the form of the current trace above approximately 10 mA, but the rise time to this current decreases from 113 ns to 60 ns with increasing I_{UV}. The change in the current trace at early time is due to the additive effect of multiple avalanches from multiple initial electrons ejected from the cathode. The 0 pA simulation was initialized with 1 electron near the cathode, and represents the limiting case of breakdown initiated by a single electron emitted from the cathode.

As I_{UV} increases from 27 pA to 2.7 nA, the initial cloud of electrons still contacts the anode at approximately the same time (30 ns), but the current at which this occurs is larger for larger I_{UV}. This larger initial current causes more excitation and more photons which reach the cathode earlier in time. As a result, the minimum in current which occurs at approximately 50 ns becomes less pronounced as I_{UV} increases. The delay before the first electron is emitted from the cathode can also cause a shift of this curve to the left or right. With a lower current, the variance in the current rise time increases because the electron emission rate varies from 1 electron every 60 ps for 2.7 nA to 1 electron every 6 ns for 27 pA. At these currents however, this effect is much less significant than the additive effect of multiple avalanches. In the 27 pA case, despite a 4 ns delay before the first electron is emitted, the current exceeds that of a 0 pA simulation (with its first electron at 0 ns) by 30 ns.

In the experiment, I_{UV} appeared to be below the detection limit of the current setup (~1 μA). Although it is possible that the value of I_{UV} in the experiment is any value below 1 μA, the smallest reasonable value was used in this paper because it provided a better agreement with the experiment (i.e., a longer rise time before the current reaches 1 mA). In the experimental data for 1.8 kV, there is a 6 ns standard deviation in the current rise time. Because the breakdown cannot begin without the first electron,

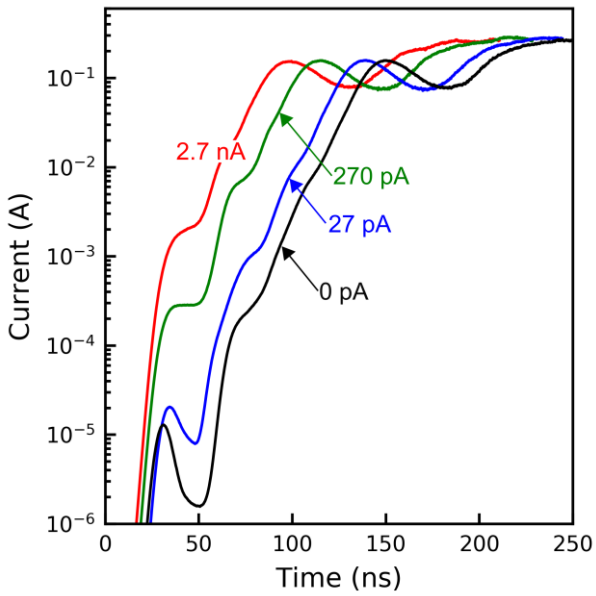

Figure 10. The current calculated in the model for varying current due to the UV diode. This is modeled as an influx of electrons from the cathode. 27 pA is the base case. The model for 0 pA was initialized with 1 electron near the cathode.

the smallest reasonable value for I_{UV} is 2.7 pA (1 e^- every 6 ns). Even choosing this minimum reasonable value, the rise time in the model is shorter than that of the experiment.

IV. Concluding Remarks

A 1D3V PIC-DSMC model was used to investigate a plane-to-plane discharge in He at 50 Torr with a Pt cathode and an external circuit. One of the main differences between the model and experimental results is that the timescales in the model are shorter. The time for the current to rise to 30 mA, and the time between the maxima in current are shorter in the model. These faster dynamics may be due to some assumptions of modeling the discharge in one dimension, the first electron being generated in the gas phase, or because the production of the first electron may be delayed by unknown effects on the surface. The rise time of the current is also highly sensitive to the initial seed electrons emitted from the cathode, which in this case were generated by shining a UV diode on the surface.

Though the experimental conditions were well controlled, the uncertainty in the condition of the surface resulted in unknown values of γ_{ph} and γ_i. Of the values we investigated, the best agreement to the experimental current measurements occurred at approximately $\gamma_{ph} = 5 \times 10^{-3}$ and $\gamma_i = 0.01$. These values are significantly below the literature values for Pt, or C which may be coating the surface. The value of γ_{ph} is underestimated in this approach because in the one-dimensional model, radial losses of photons are ignored, leading to a larger flux of photons than would occur in a three-dimensional simulation. The estimated value for γ_i of 0.01 is between the experimental value for a pristine and "dirty" Pt surface [7].

By varying the secondary electron yields, their effect on the current has been demonstrated. Increasing γ_{ph} causes the current to rise faster after the initial time for the electrons to transit the gap (~30 ns) and increases the amplitude of the first peak in the discharge current. Increasing γ_i increases the maximum current which is reached before a drop in the applied voltage due to the driving circuit limits the current. Many plasma models do not include γ_{ph}. These results indicate that excluding the photoelectron emission will result in an artificially slow current rise, although it may still be possible to capture the steady state or maximum current using only γ_i. Better understanding of the role of these material properties will aid in the selection of electrode materials for various applications.

Acknowledgements
The authors are grateful to Michael Brumbach for surface characterizations which helped inform this investigation. Supported by the Laboratory Directed Research and Development program at Sandia National Laboratories, a multi-mission laboratory managed and operated by National Technology and Engineering Solutions of Sandia LLC, a wholly owned subsidiary of Honeywell International Inc. for the U.S. Department of Energy's National Nuclear Security Administration under contract DE-NA0003525. This paper describes objective technical results and analysis. Any subjective views or opinions that might be expressed in the paper do not necessarily represent the views of the U.S. Department of Energy or the United States Government.

References

[1] A. Fierro, E. Barnat, C. Moore, M. Hopkins and P. Clem, "Kinetic simulation of a low-pressure helium discharge with comparison to experimental measurements," *Plasma Sources Sci. Technol.,* vol. 28, no. 055012, 2019.

[2] X. Yao, N. Jiang, B. Peng, Y. Xia, N. Lu, K. Shang, J. Li and Y. Wu, "DC discharge with high secondary electron emission oxide cathode: Effects of gas pressure and oxide cathode structure," *Vacuum,* vol. 166, pp. 114-122, 2019.

[3] A. M. Lietz, E. V. Barnat, J. E. Foster and M. J. Kushner, "Ionization wave propagation in a He plasma jet in a controlled gas environment," *J. Appl. Phys.,* vol. 128, no. 083301, 2020.

[4] Z. Wu, G. Sun, S. Yuan, T. Huang, X. Liu, K. Xie and N. Wang, "Discharge reliability in ablative pulsed plasma thrusters," *Acta Astronautica,* vol. 137, pp. 8-14, 2017.

[5] A. Dunaevsky, Y. Raitses and N. J. Fisch, "Secondary electron emission from dielectric materials of a Hall thruster with segmente delectrodes," *Phys. of Plasmas,* vol. 10, no. 6, 2003.

[6] X. Yao, N. Jiang, J. Li, N. Lu, K. Shang and Y. Wu, "An improved corona discharge ignited by oxide cathodes with high secondary electron emission for toluene degradation," *Chem. Eng. J.,* vol. 362, pp. 339-348, 2019.

[7] A. V. Phelps and Z. L. Petrović, "Cold-cathode discharges and breakdown in argon: surface and gas phase production of secondary electrons," *Plasma Sources Sci. Technol.,* vol. 8, pp. R21-R44, 1999.

[8] M. M. Nikolić, A. R. Dordević, I. Stefanović, S. Vrhovac and Z. L. Petrović, "Semianalytical models of volt-ampere characteristics of diffuse low-current low-pressure discharges," *IEEE Trans. Plasma Sci.,* vol. 31, no. 4, 2003.

[9] D. Maric, M. Savic, J. Sivos, N. Skoro, M. Radmilovic-Radjenovic, G. Malovic and Z. L. Petrovic, "Gas breakdown and secondary electron yields," *Eur. Phys. J. D,* vol. 68, no. 155, 2014.

[10] M. Daksha, B. Berger, E. Schuengel, I. Korolov, A. Derzsi, M. Koepke, Z. Donko and J. Schultze, "A computationally assisted spectroscopic technique to measure secondary electron emission coefficients in radio frequency plasmas," *J. Phys. D: Appl. Phys.,* vol. 49, no. 234001, 2016.

[11] Z. L. Petrović, Z. Donko, D. Marić, G. Malović and S. Zivanov, "CCD images of low-pressure low-current DC discharges," *IEEE Trans. Plasma Sci.,* vol. 30, no. 1, 2002.

[12] H. E. Delgado, D. T. Elg, D. M. Bartels, P. Rumbach and D. B. Go, "Chemical analysis of secondary electron emission from a water cathode at the interface with a nonthermal plasma," *Langmuir,* vol. 36, pp. 1156-1164, 2020.

[13] M. M. Pejović, M. M. Pejović and K. Stanković, "Experimental investigation of breakdown voltage and electrical breakdown time delay of commercial gas discharge tubes," *Jpn. J. of Appl. Phys.,* vol. 50, no. 086001, 2011.

[14] C. A. Maluckov, S. A. Rančev and M. K. Radović, "Applying the different statistical tests in analysis of electrical breakdown mechanisms in nitrogen filled gas diode," *Plasma Sci. Technol.,* vol. 18, no. 10, 2016.

[15] V. L. Marković, Z. L. Petrović and M. M. Pejović, "Surface recombination of atoms in a nitrogen afterglow," *J. Chem. Phys.,* vol. 100, no. 8514, 1994.

[16] G. Bird, Molecular Gas Dynamics and the Direct Simulation of Gas Flows, Oxford: Oxford University Press, 1994.

[17] M. A. Heroux and J. M. Willenbring, "A new overview of the Trilinos project," *Sci. Program.,* vol. 20, p. 83, 2012.

[18] A. Fierro, C. Moore, B. Scheiner, B. T. Yee and M. M. Hopkins, "Radiation transport in kinetic simulations and the influence of photoemission on electron current in self-sustaining discharges," *J. Phys. D: Appl. Phys.,* vol. 50, no. 065202, 2017.

[19] S. Ramo, "Currents Induced by Electron Motion," *Proceedings of the I.R.E.,* p. 584, 1939.

[20] W. Shockley, "Currents to conductors induced by a moving point charge," *J. Appl. Phys.,* vol. 9, p. 635, 1938.

[21] P. N. Giuliano and I. D. Boyd, "Modeling particle-induced electron emission in a simplified plasma Test Cell," *J. Appl. Phys.,* vol. 113, no. 113302, 2013.

[22] H. Helm, "The cross section for symmetric charge exchange of He+ in He at energies between 0.3 and 8 eV," *J. Phys. B: Atom. Molec. Phys.,* vol. 10, no. 18, 1977.

[23] A. Fierro, J. Lehr, B. Yee, E. Barnat, C. Morre, M. Hopkins and P. Clem, "Study of vacuum ultraviolet emission in helium and helium/nitrogen mixtures," *J. Appl. Phys.,* vol. 129, no. 073302, 2021.

[24] N. A. Roberds, M. M. Hopkins, B. T. Yee, A. Fierro and C. H. Moore, "Modeling DC electrical breakdown using a truncated emission spectrum for trapped radiation," *Phys. Plasmas,* vol. 27, no. 043507, 2020.

[25] A. F. Molisch and B. P. Oehry, Radiation Trapping in Atomic Vapours, Oxford: Oxford University Press, 1998.

[26] A. E. Siegman, Lasers, Mill Valley: University Science, 1986.

[27] Z. Eckert, J. J. Boerner and A. M. Grillet, "1D PIC-DSMC analysis of a high-pressure nanosecond pulse discharge breakdown in helium," *J. Phys. D: Appl. Phys.,* vol. 53, no. 035203, 2020.

[28] Y. Razier, Gas Discharge Physics, Springer, 1997.

[29] B. Feuerbacher and B. Fitton, "Experimental Investigation of photoemission from satellite surface materials," *J. Appl. Phys.,* vol. 43, no. 1563, 1972.

[30] W. Choi, C. Kim and H. Kang, "Interactions of low energy (10-600 eV) noble gas ions with a graphite surface: surface penetration, trapping and self-sputtering behaviors," *Surf. Sci.,* vol. 281, pp. 323-335, 1993.